Compositional Mapping of Europa and Ganymede with VLT/SPHERE and Galileo/NIMS using Markov Chain Monte Carlo Fitting. O. R. T. King[1] and L. N. Fletcher[1], [1]School of Physics and Astronomy, University of Leicester, Leicester, LE1 7RH, UK (ortk1@le.ac.uk, leigh.fletcher@le.ac.uk),

Introduction: The Galilean satellites' surfaces and subsurfaces will be explored by robotic spacecraft in the late 2020s and early 2030s, but significant advances from ground-based astronomical facilities will be possible in the coming decade. Europa's surface is composed of water ice, with significant contamination from sulfuric acid hydrates and potentially hydrated salts [2,10]. Ganymede's surface is composed of regions of brighter young terrain with similar composition to Europa, and older dark terrain which has a higher abundance of silicate rich material [11,16]. Infrared spectra from the Galileo orbiter Near-Infrared Mapping Spectrometer (NIMS) provided high spatial resolution IR spectra of Europa and Ganymede but with limited spatial coverage in many locations. In recent years, ground-based adaptive optics observations in the infrared with Keck/OSIRIS and VLT/SINFONI have provided new insights into the distributions of surface materials on Europa and Ganymede [2,4,10,11].

Datasets: Near-IR observations of Europa and Ganymede were taken during VLT/SPHERE [1] science verification in 2014 and 2015. These observed Europa's anti-jovian hemisphere (sub-observer longitude of 192°W) and Ganymede's leading/anti-jovian hemisphere (sub-observer longitude of 116°W). Data were taken in IRDIFS_EXT mode, allowing simultaneous imaging with the Integral Field Spectrograph (IFS) and Infrared Differential Imaging Spectrometer (IRDIS) sub-systems of the SPHERE instrument. IFS [5,13] produces image cubes with spectra from 0.95 to 1.65 µm (R~30). It has a high spatial resolution, with a pixel size of 7.46 mas/px, corresponding to ~25 km/px at Jupiter. Accounting for diffraction, this allows features ~150 km across to be resolved. For example, Europa's largest lineae are resolved in Figure 1, the first time this has been possible from Earth. IRDIS produced simultaneous imaging through two filters, with transmissions centred on 2.11 and 2.25 µm which enables measurement of the strength of water ice absorption around 2 µm. We have also analysed a series of Galileo/NIMS observations with similar spectral and spatial coverage to our SPHERE data. The NIMS detector covering the 0.99 to 1.26µm wavelength range failed early in the Galileo mission at Jupiter, meaning the NIMS coverage of the SPHERE spectral range is limited.

The datasets have been reduced and cleaned to produce mapped spectral cubes of Europa and Ganymede's observed hemispheres. Images are photometrically corrected to remove the variation in brightness towards the edge of the observed disc caused by varying viewing angles and illumination levels of the surface. Our photometric correction uses the Oren-Nayar model, which generalizes the Lambertian model to more accurately represent rough surfaces [15]. This enables regions at large emission angles to be mapped accurately, providing significant improvements over the Lambertian model which overcorrects the brightness towards the edge of the disc. The Oren-Nayar correction allows our mapping to reach emission angles ~70°, higher than previous studies that extend to 50° to 60° [2,7,10].

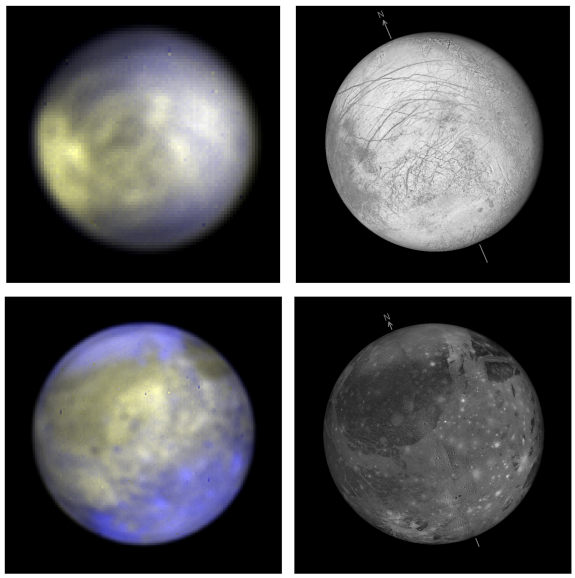

Figure 1: Two-colour images of IRDIS observations (left) of Europa (top) and Ganymede (bottom), yellow is 2.11 µm and blue is 2.25 µm, compared to simulated visible light images (right). Water ice has a broad absorption band around 2µm, so the blue areas are icy and yellow areas dominated by non-icy species. Large observed features include the icy poles of both moons, Europa's contaminated trailing hemisphere and the clear contrast between Ganymede's older dark regions and younger icier terrain.

Spectral modelling: We analyse the mapped cubes by fitting to laboratory spectra from reference cryogenic libraries. These reference spectra include water ice, sulfuric acid, and hydrated salts [3,8,12]. We have developed an implementation of the Hapke bidirectional reflectance model [9] which we use to model a range of ice grain sizes.

Our fitting routine is run for each observed location to produce compositional maps of Europa's anti-jovian hemisphere. We treat each observed spectrum as a linear combination of discrete endmembers $E_i(\lambda)$ with respective abundances a_i, where the modelled spectrum is calculated as $M(\lambda) = \sum_i a_i E_i(\lambda)$. Our routine uses Markov Chain Monte Carlo techniques [6] to model an observed spectrum, producing a posterior distribution of fitted abundance values for each endmember, and combinations of different endmembers (Figure 2).

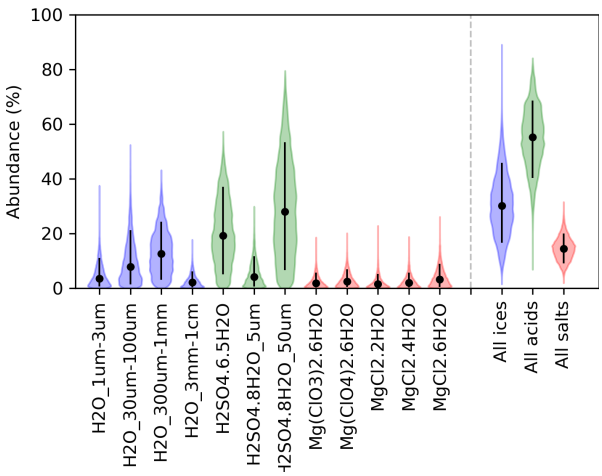

Figure 2: Example fitting results using our Monte Carlo fitting routine on a non-icy location on Europa. The black dots give the best estimate abundance and the lines show the 1-sigma range. The width of the coloured area is representative of the posterior distribution of that endmember's abundance.

The median of each distribution is used as the best estimate abundance for each endmember, and the width of the distribution is used to estimate the uncertainty on that central value. The posterior distributions of combinations of endmembers can likewise be calculated, accounting for correlations in the uncertainties of the summed endmembers. Whilst the uncertainty on a specific endmember's abundance may be large (e.g., a specific ice grain size), the uncertainty of the abundance of a combination of endmembers is often much smaller (e.g., the total abundance of all ice endmembers).

The use of Monte Carlo techniques allows better exploration of the endmember parameter space than a simple linear fit, and the uncertainty estimates allow more detailed understanding of potential detections.

Modelling results from the SPHERE and NIMS Europa datasets show strong similarities and are consistent with previously observed compositional features. These include the leading-trailing hemisphere difference in water ice fraction and the structure of non-ice material (mainly sulfuric acids) from the anti-jovian point to Powys Regio. Salts have a lower abundance and appear spatially constrained to geological features including Dyfed and Powys Regio, and the region around the northern hemisphere lineae.

Additional SPHERE observations were planned to achieve full longitude coverage of Europa and Ganymede in 2020, however this observing campaign has been delayed due to the COVID-19 pandemic. This full observing campaign will allow ~95% of Europa and Ganymede's surface areas to be mapped using SPHERE.

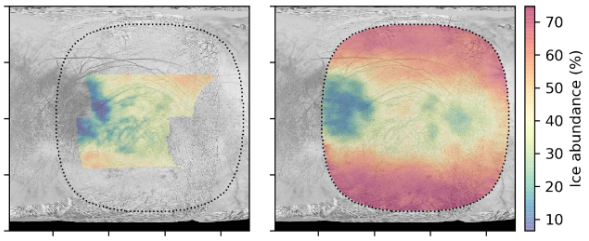

Figure 3: Example fit result of Galileo/NIMS (left) and VLT/SPHERE (right) observations of Europa's anti-jovian hemisphere produced by our fitting routine.

Acknowledgments: We would like to thank the Royal Society for supporting this work.

References: [1] Beuzit et al 2019, arXiv: 1902.04080. [2] Brown & Hand 2013, The Astronomical Journal, 145(4):110. [3] Carlson, Johnson, & Anderson, 1999, Science, 286(5437):97–99. [4] Carlson et al., 1992, The Galileo Mission, pages 457–502. Springer. [5] Claudi et al., 2008: Ground-based and Airborne Instrumentation for Astronomy II, volume 7014, page 70143E. International Society for Optics and Photonics, SPIE. [6] Foreman-Mackey et al., 2013, Publications of the Astronomical Society of the Pacific 125(925):306. [7] Grundy et al., 2007, Science, 318(5848):234–237. [8] Hanley et al., 2014, Journal of Geophysical Research: Planets, 119(11):2370–2377.[9] Hapke, 1993, Theory of reflectance and emittance spectroscopy, Cambridge University Press. [10] Ligier et al., 2016, The Astronomical Journal, 151(6):163. [11] Ligier et al., 2019, Icarus, 333:496-515. [12] McCord et al., 1999, Journal of Geophysical Research: Planets, 104(E5):11827–11851. [13] Mesa et al., 2015, Astronomy & Astrophysics, 576:A121. [15] Oren & Nayar, 1944, Proceedings of the 21st annual conference on Computer graphics and interactive techniques, pages 239–246. ACM. [16] Pappalardo et al., 2004, Jupiter: The Planet, Satellites and Magnetosphere, 363-396.